ISSN PRINT 2319 1775 Online 2320 7876

 UGC CARE Listed ( Group -I) Journal Volume 11, Iss 01, 2022

# Numerical Study of V-ribs on the Performance of Flat Plate Solar Air Heater for Food Drying Applications

**Satish Kumar Gavel[1], Sandip Kumar Sahu[2], Avinash Ranjan Patnaik[3], Praveen Kumar Kujur[4],Uday Khakha[5], Aditya Singh[6], Shyam Singh Kanwar[7], Rahul Gupta[8]**

[1,2,3,4,5,7]Assistant Professor, Department of Mechanical Engineering, Government Engineering College, Bilaspur, C.G, India[6]Assistant Professor,Department of Civil Engineering, Government Engineering College, Bilaspur, C.G, India

[8]Assistant Professor, Department of Electronics & Telecommunication Engineering, Government Engineering College, Bilaspur, C.G, India

[1]gavel.satish@gmail.com, [7]shyamkanwar@gecbsp.ac.in

**Submission date: 15 December 2021 accepted date: 05 January 2022. Publication date: 25 January 2022.**

**ABSTRACT**

Drying of foods and grains are done for food preservation. It prevents growth of bacteria, yeasts and other microorganisms through removal of water content from it. The utilization of artificial roughness, such as ribs, on the underside of the absorber plate of a solar air heater (SAH) has been widely recognized as an effective method to enhance its thermal performance. Various experimental and computational studies have been conducted to enhance heat transfer from the absorber plate to the flowing air in SAH systems. This study presents a computational investigation into the impact of employing V-ribs as roughness elements on the heat transfer coefficient and friction factor of SAH. Additionally, an analysis is performed to assess the influence of flow direction relative to the absorber plate on heat transfer and friction factor. The study considers parameters such as Reynolds Number (Re) ranging from 2000 to 20000, relative roughness width (W/w) of 1, relative roughness pitch (P/e) of 10, relative roughness height (e/D) of 0.043, and an angle of attack (α) of 30°. The results indicate that the incorporation of V-ribs as artificial roughness in the SAH leads to increased Nusselt Number and friction factor compared to a smooth SAH, attributed to enhanced turbulence. The hot outlet air which is in the temperature range of 300 K to 355 K can be utilized for the drying of various foods, vegetables and grains.

***Keywords:****Solar air heater, V-ribs, Flat Plate collector, Ansys Fluent, Computational Study, Food Grain Drying.*

## 1. INTRODUCTION

Since 1973, energy has been a recurrent topic in the news, particularly due to steep increases in oil prices and shortages worldwide. It's evident that the era of fossil fuels, our non-renewable energy resources, is gradually drawing to a close. Natural gas and oil are expected to be depleted first, followed eventually by coal. However, there are numerous alternative energy sources that can replace fossil fuels. The decision regarding which energy source to utilize in each case must consider safety, economic factors, and environmental impacts. Due to its

ISSN PRINT 2319 1775 Online 2320 7876

 UGC CARE Listed ( Group -I) Journal Volume 11, Iss 01, 2022

favorable safety and environmental aspects, solar energy is widely regarded as a preferable alternative. Essentially, all other forms of energy originate from the sun. Oil, coal, wood, and natural gas were initially produced through photosynthesis, followed by subsequent chemical reactions involving decaying vegetation subjected to high pressure and temperature over time.

Solar energy can be utilized both directly and indirectly in various thermal applications, such as heating water and air, drying air and water, distillation, and cooking. The heated fluid can serve multiple purposes, including power generation and refrigeration. This study focuses solely on the thermal energy conversion of solar energy.

Various researchers have conducted experimental investigations on enhancing the thermal performance of solar air heaters using different roughness elements. For instance, Hans et al. [3] studied the impact of multiple V-rib roughness on heat transfer coefficient and friction factor in a solar air heater duct. Gupta et al. [4] examined the effects of transverse wire roughness on fluid and heat flow characteristics in solar air heater ducts. These studies collected experimental data and developed correlations for friction factor and Nusselt Number based on roughness geometry and flow parameters.

Other researchers explored different roughness configurations, such as rib-grooved roughness [8], arc-shaped parallel wire roughness [11], dimple-shaped ribs [12], inverted-shaped ribs [13], and W-shaped ribs [15][16]. These studies investigated the effects of various operating parameters on heat transfer and friction factor, comparing results with smooth duct conditions.

Additionally, numerical simulations have been employed to investigate the thermal and hydraulic performance of solar air heater ducts roughened with non-uniform cross-section square wave profile transverse ribs [17], further contributing to our understanding of optimizing solar energy utilization.

## 2. METHODOLOGY

### 2.1 Description of problem

In this study, a duct with dimensions of 1000mm length, 300mm width, and 25mm height is utilized. The hydraulic diameter of the duct is calculated as 46.15mm. One side of the duct is deliberately roughened using artificial ribs, while the other three sides remain smooth and insulated. The investigation focuses on the impact of V-shaped ribs on the performance of a Flat Plate Solar Air Heater (FPSAH) compared to a smooth duct configuration. Specifically, the study employs square wave profile with multiple V-shaped ribs, set at an angle of attack (α) of 30° from the inlet. The investigation aims to understand how these artificial V-Ribs affect the performance of the FPSAH in comparison to a smooth duct. The geometries of both the smooth duct and the duct with artificial V-Ribs are depicted in Figure 1 and Figure 2, respectively. In the initial phase of our study, we analyze the performance of a smooth duct with axial air inlet flow, utilizing the geometry as illustrated in Figure 1.

ISSN PRINT 2319 1775 Online 2320 7876

 CARE Listed ( Group -I) Journal Volume 11, Iss 01, 2022

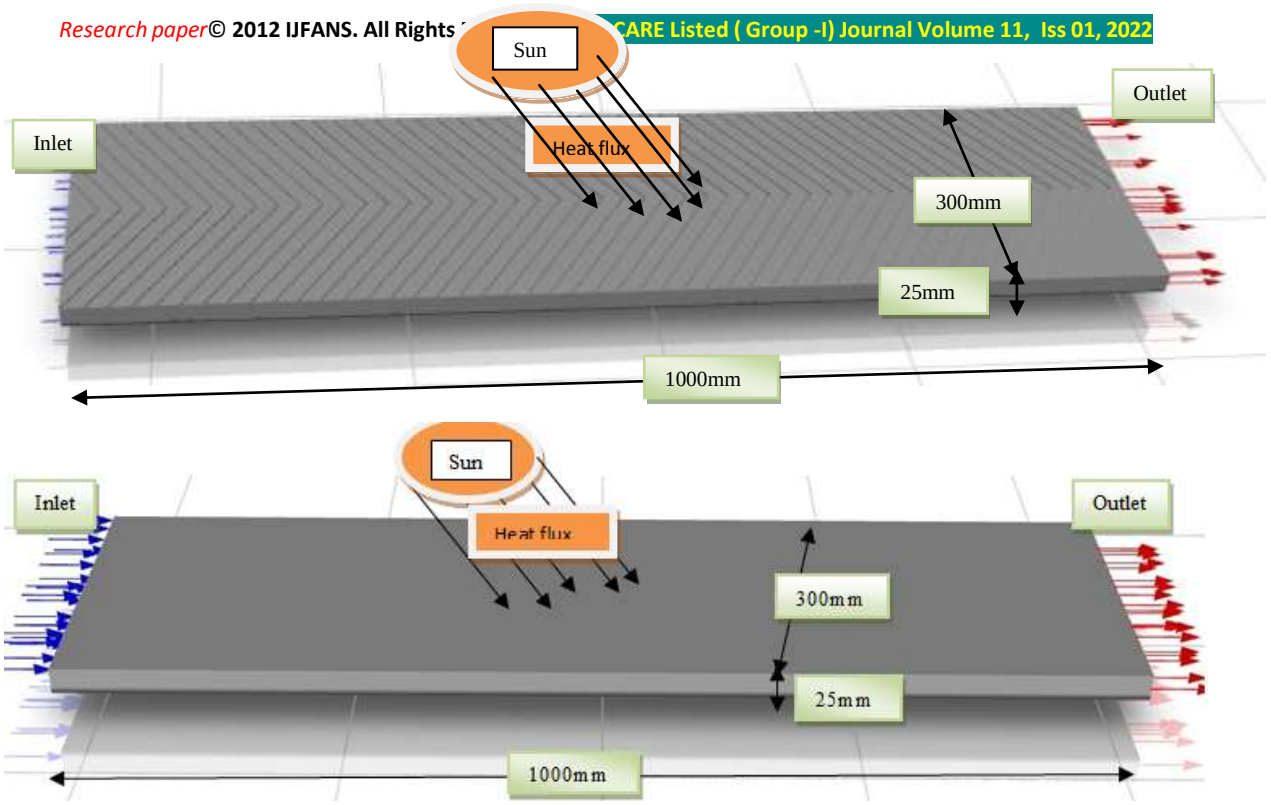


Figure 1: Geometryof Smooth duct.

In the present study (roughened duct as V-ribs ), is taken. Here the direction of air flow for inlet and outlet is axial. The geometry size is same as that of smooth duct and shown in figure 2.

Figure 2:Geometryof Smooth duct with multi V-ribs.

The ribs size is 2mm in width and 2mm in height. Figure 3 gives the dimensions of the rib geometry.

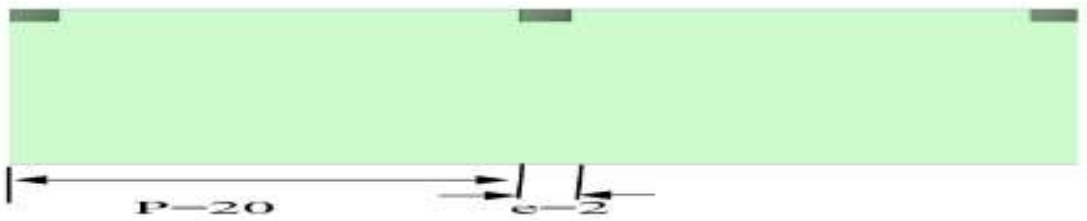


Figure 3: Rib dimension (in mm) between two consecutive ribs

ISSN PRINT 2319 1775 Online 2320 7876

 UGC CARE Listed ( Group -I) Journal Volume 11, Iss 01, 2022

The range of roughness and operating parameters are given in table below.

| S.no. | Roughness parameters | Range |
|---|---|---|
| 1. | Reynolds Number, Re | 2000-20000 (10 values) |
| 2. | Relative roughness height, e/D | 0.043 |
| 3. | Relative roughness Width, W/w | 1 |
| 4. | Relative roughness pitch, P/e | 10 |
| 5. | Angle of attack, α | 30° |

Table 1: Range of roughness and operating parameters [3]

Reynolds Number for the flow in the collectors is calculated using their hydraulic diameter i.e. 46.15 mm.

### 2.2 Governing Equations

The averaged conservative equations under the present situation can be written as follows:

**Conservation of mass equation**

$$\frac{\partial(\rho u)}{\partial x}+\frac{\partial(\rho v)}{\partial y}+\frac{\partial(\rho w)}{\partial z}=0 \quad \text{.....(1)}$$

**Energy equation**

$$\rho C_p\left(u\frac{\partial T}{\partial x}+v\frac{\partial T}{\partial y}+w\frac{\partial T}{\partial z}\right)=k\left(\frac{\partial^2 T}{\partial x^2}+\frac{\partial^2 T}{\partial y^2}+\frac{\partial^2 T}{\partial z^2}\right) \quad \text{.....(2)}$$

**Conservation of momentum equation**

$$u\frac{\partial(\rho u)}{\partial x}+v\frac{\partial(\rho u)}{\partial y}+w\frac{\partial(\rho u)}{\partial z}=-\frac{\partial p}{\partial x}+\mu\left(\frac{\partial^2 u}{\partial x^2}+\frac{\partial^2 u}{\partial y^2}+\frac{\partial^2 u}{\partial z^2}\right) \quad \text{.....(3)}$$

$$u\frac{\partial(\rho v)}{\partial x}+v\frac{\partial(\rho v)}{\partial y}+w\frac{\partial(\rho v)}{\partial z}=-\frac{\partial p}{\partial y}+\mu\left(\frac{\partial^2 v}{\partial x^2}+\frac{\partial^2 v}{\partial y^2}+\frac{\partial^2 v}{\partial z^2}\right) \quad \text{.....(4)}$$

$$u\frac{\partial(\rho w)}{\partial x}+v\frac{\partial(\rho w)}{\partial y}+w\frac{\partial(\rho w)}{\partial z}=-\frac{\partial p}{\partial x}+\mu\left(\frac{\partial^2 w}{\partial x^2}+\frac{\partial^2 w}{\partial y^2}+\frac{\partial^2 w}{\partial z^2}\right) \quad \text{.....(5)}$$

Some other equations for solving our problem are given below.

**Useful Heat Gain**

$$Q_u = mC_p(T_o - T_i)$$

**Convective heat transfer coefficient**

$$h = \frac{Q_u}{A_c(T_p - T_f)}$$

**Nusselt Number**

$$\overline{Nu} = \frac{\bar{h}D}{k}$$

ISSN PRINT 2319 1775 Online 2320 7876

 UGC CARE Listed ( Group -I) Journal Volume 11, Iss 01, 2022

**Friction Factor**

$$f = \frac{2\Delta P_d D}{4\rho L v^2}$$

For validity test of friction factor and Nusselt Number to determine from experimental data for smooth duct have been compared with the value obtained from Modified Blasius Equation and Dittus Boelter Equation for Nusselt Number and friction factor, respectively.

**Modified Blasius Equation**

$$f_s = 0.085Re^{-0.25}$$

**Dittus Boelter Equation**

$$Nu_s = 0.023Re^{0.8}P^{0.4}$$

**2.3 Solution Method**

In this section, framework to solution method has been discussed. Following are the assumptions taken in present study.

- Study is based on 3 dimensional geometrical models.
- Air is taken as incompressible.
- Flow is steady and turbulent.

**2.3.1 Geometry Formation**

In this section, we outline the methodology employed for creating the geometries using Space Claim software.For the first study involving a smooth duct with axial air inlet flow, we begin by creating a rectangle with dimensions of 1000mm in length and 25mm in height. This rectangle is then extruded to a width of 300mm, resulting in our basic smooth duct geometry, as depicted in Figure 1. For the second study, focusing on a roughened duct with V-ribs and axial air inlet flow, we follow a similar process. After creating the duct shape, we proceed to generate the ribs on the absorber plate using the line command to create V-rib shapes with dimensions of 2mm×2mm at a 30° angle. Subsequently, we use the pull command with the cutting option to extrude the ribs into the duct, resulting in 2mm×2mm cutouts on the absorber plate. Utilizing the patterning option, we replicate these ribs across the absorber plate to achieve the final geometry for the second study, as depicted in Figure 2 and Figure 3.

**2.3.2 Meshing of Geometry**

To obtain solutions for real flows, a numerical approach must be adopted whereby the equations are replaced by algebraic approximations which may be solved using a numerical method, by using the approach of 'Discretization of the Governing Equations' involves fragmenting the spatial domain into small finite control volumes using a mesh.

Here the meshing is done by taking the elemental size of 4.5mm and we get the nodes of 104453 and the meshing elements for this are 470000.

ISSN PRINT 2319 1775 Online 2320 7876

 UGC CARE Listed ( Group -I) Journal Volume 11, Iss 01, 2022

Figure 4: Meshing of the geometry

### 2.3.3 Turbulence Model

The Standard k-ε Model is a simplest two equations model for the variables k and ε i.e., turbulent kinetic energy and its dissipation effects are generally preferred to find the value of the turbulent velocity and length scales. Now the Standard k-ε Model is a role model for different types of problems because it is simple and takes less computational time and also gives the accurate results. Two transport equations for the turbulence kinetic energy (k) and turbulence kinetic energy dissipation rate (ε) are used with this model. Two transport equations for the turbulence kinetic energy (k) and its dissipation rate (ε) are derived with the help of physical and mathematical interpretation. In the present study standard k- ε model was only preferred to solve the flow problems, which are totally turbulent in nature. In this model the effect of molecular viscosity is not taken in to consideration.

### 2.3.4 Boundary conditions and fluid properties

**a) Inlet boundary conditions**

- Types of boundaries - Velocity-inlet (5 different location)
- Reynolds number –2000-20000 (10 values)

**b) Outlet boundary conditions**

- Types of boundaries - Pressure-outlet
- Pressure-specified - 0 Pa (Gauge)

**c) Wall boundary conditions**

- Heated wall - Heat flux (Q-1000 W/$m^2$)
- Insulated wall - 3 side are insulated

**d) Working fluid properties**

- Working fluid – Air
- The density of working fluid - 1.225 kg/$m^3$
- Viscosity of working fluid -1.78 × $10^{-5}$ kg/m-s
- Element shape of meshing- Quad/triangular

## 3. RESULTS & DISCUSSIONS

In this section, we delve into the analysis of air attributes by plotting static pressure, temperature, and velocity profile contours across all 10 Reynolds Numbers ranging from 2000 to 20000. Initially, validation work is conducted to ensure the accuracy of the computational results by comparing them with experimentally obtained

ISSN PRINT 2319 1775 Online 2320 7876

*Research paper*, **UGC CARE Listed ( Group -I) Journal Volume 11, Iss 01, 2022**

results from Hans VS, Saini RP, and Saini JS [3]. This validation process aims to assess grid independence and determine the most suitable model for the present investigation based on the degree of agreement between computational and experimental results in terms of inlet flow conditions, development of velocity profile, and changes in temperature and pressure drop.

The quality of meshing chosen significantly influences the outcomes of any numerical turbulence model, whether it's coarse, fine, or the finest, for a given 3D geometry. Meshing involves dividing the computational domain into small regions, typically consisting of nodes, cells, and grids. The results of computational models are intricately tied to the size and structure of the grid. In our study, meshing is performed with an elemental size of 4.5mm, resulting in 104453 nodes and 470000 meshing elements. This meshing strategy aims to accurately capture the intricate details of the physical problem under investigation.

**3.2 Smooth Duct and duct with multi V-ribs**

It is very difficult to choose an optimum turbulence model due to variations of physical conditions in various processes where we have to handle different types of Parameters. An optimum model is a model which gives the results very close to the experimental results under given conditions. So, in this study Standard k–ε turbulence model is used to obtain the required parameters.

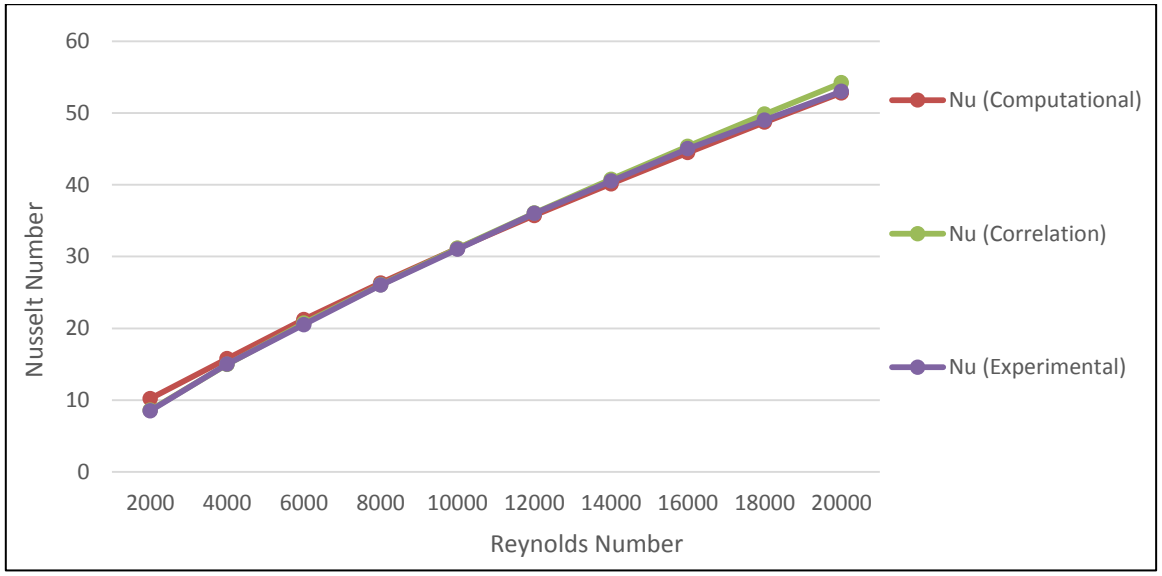


Figure 5: Variation of Nusselt No. with Reynolds No. for smooth duct.

In figure 5 result of Nusselt Number with respect to different Reynolds Number for smooth duct and duct with roughness are presented. It can be clearly seen that, when we increase the value of Reynolds Number from 2000 to 20000, the value of Nusselt number for smooth duct increases. It can also be observed that the present computational study results have very good matching with experimental results [3] and the result obtained by correlation.

ISSN PRINT 2319 1775 Online 2320 7876

 **UGC CARE Listed ( Group -I) Journal Volume 11, Iss 01, 2022**

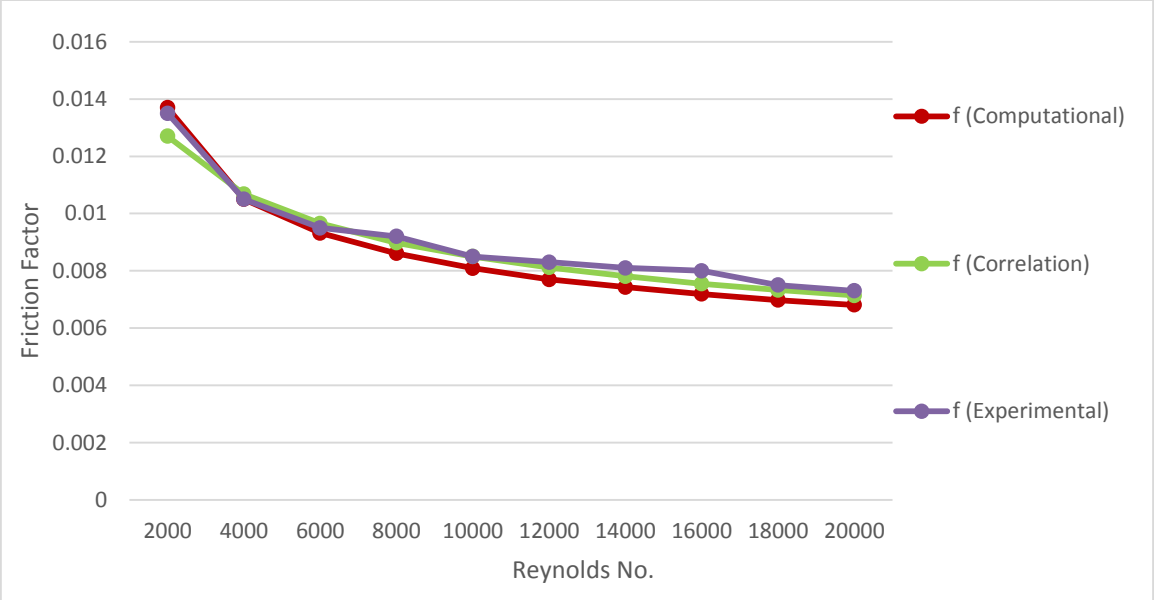


Figure 6: Variation of Friction factor with Reynolds no. for smooth duct.

In figure 6 variation of friction factor with Reynold Number for the smooth duct is shown and compared with the results of exaperimental work [3] and the friction factor data from correlation. It can be observed that the present computational results have got fairly good consistency with experimental and correlation data.

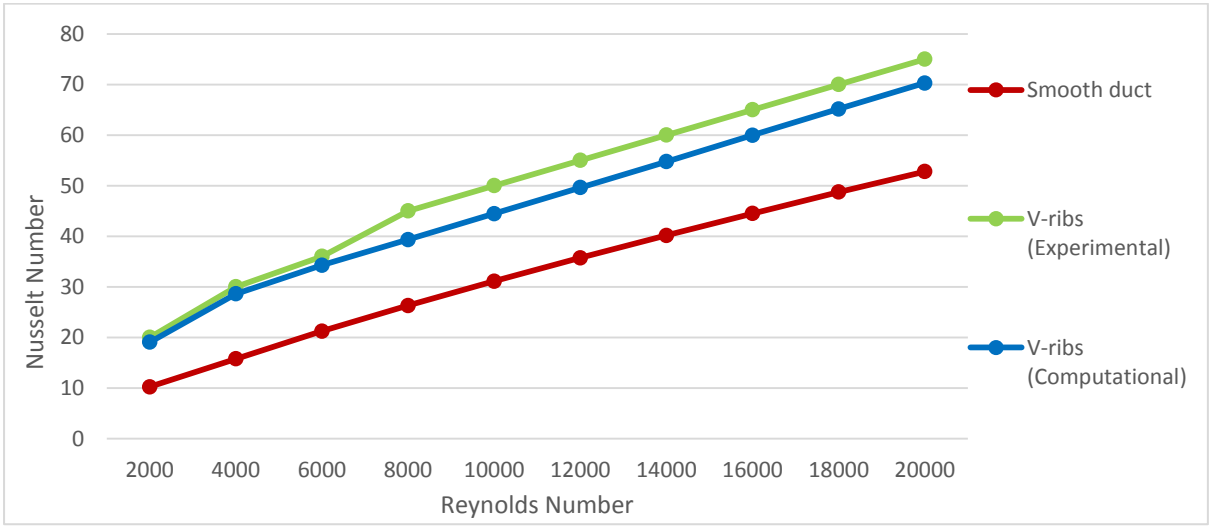


Figure 7: Variation of Nusselt No. with Reynolds no. for V-ribs duct.

Figure 7 presents the variation of Nusselt Number with Reynolds Number for smooth as well as roughened duct. Here it can be seen that due to increase in roughness the Nusselt Number consequently the heat transfer has increased as compared to that of smooth duct. It can also be noted that present computational and experimental results [3] have fairly good consistency.

ISSN PRINT 2319 1775 Online 2320 7876

 UGC CARE Listed ( Group -I) Journal Volume 11, Iss 01, 2022

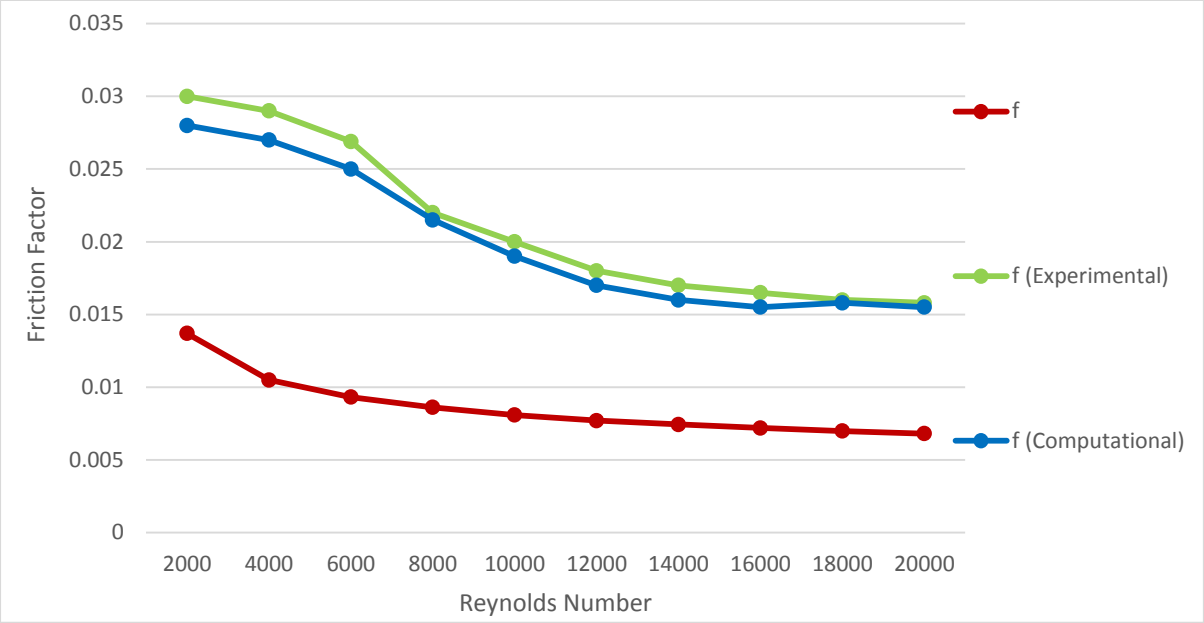


Figure8: Variation of Friction factor with Reynolds No.

Figure 8 shows the variation of friction factor with Reynolds Number for smooth as well as roughened duct. Here it can be seen that due to increase in roughness the Number consequently the pressure loss across the duct has increased as compared to that of smooth duct. It can also be noted that present computational and experimental results [3] have fairly good consistency.

Reynolds Number increases from 2000 to 20000, there is a corresponding increase in Nusselt Number across all duct geometries.

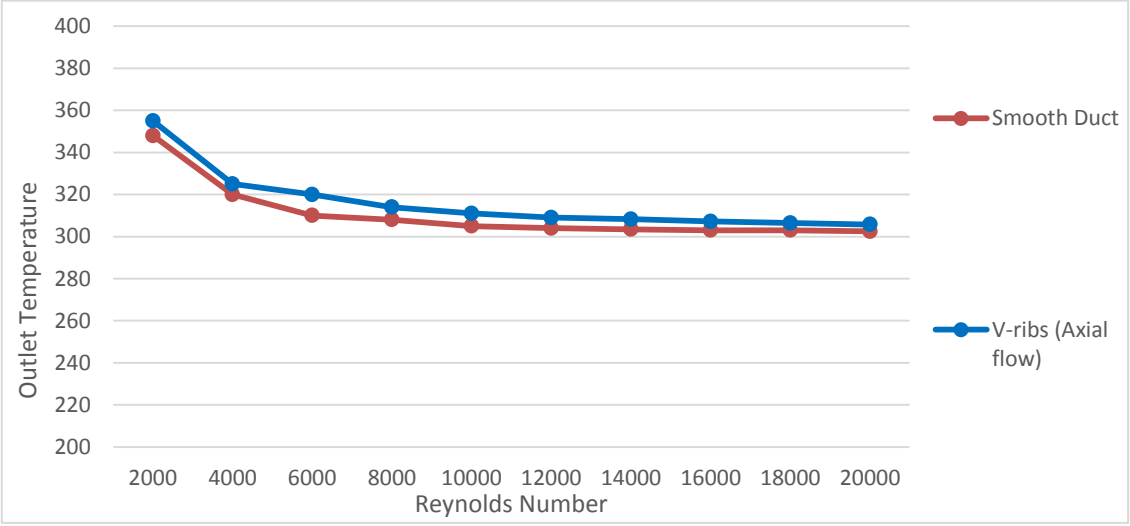


Figure 9: Variation of Outlet Air Temperature with Reynolds No.

In figure 9the variation of air outlet temperature is presented with Reynolds Number varying from 2000 to 20000. It can be seen clearly that by increase in Reynolds Number outlet air temperature decreases due to increase in mass flow rate. However for that same Reynolds Number outlet air temperature is higher for multi

ISSN PRINT 2319 1775 Online 2320 7876

*Research paper*, **UGC CARE Listed ( Group -I) Journal Volume 11, Iss 01, 2022**

V-rib roughened duct as compared to that of smooth duct. The maximumoutlet temperature obtained here is 355 K for the V-rib roughened duct corresponding to Reynolds Number of 2000. However the inlet air temperature taken here is 300 K. This hot air can be suitably used for drying of various food materials, vegetables and grains.

**3.3 Pressure contours, temperature contours, velocity contours**

The figures 10 to figure 15 illustrate the distribution of static pressure contours, temperature contours, and velocity contours across the smooth as well as the duct with artificial roughness in the form of multi V-ribs. These contours are visualized to provide insight into the pressure, temperature, and velocity variations within the duct.

**3.3.1 Pressure contours**

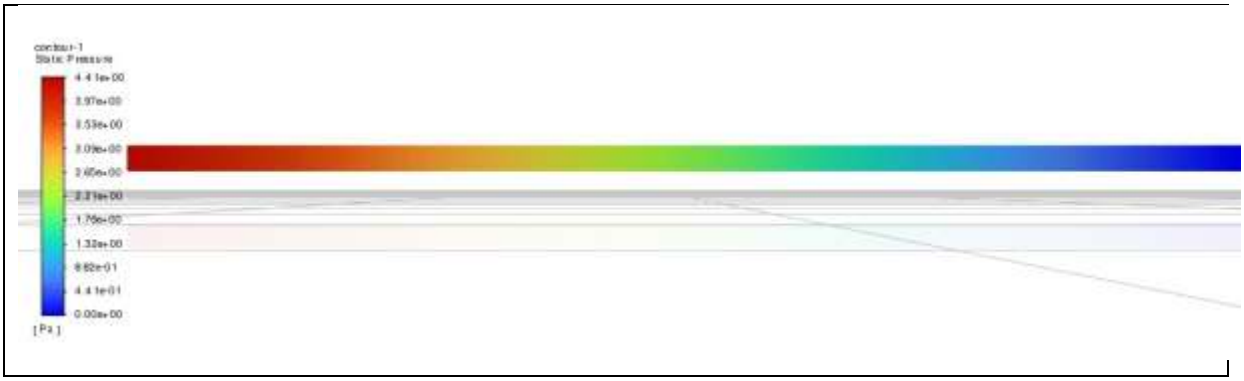

Figure 10: Pressure contour at Re=10000 of SAH Smooth duct axial air flow.

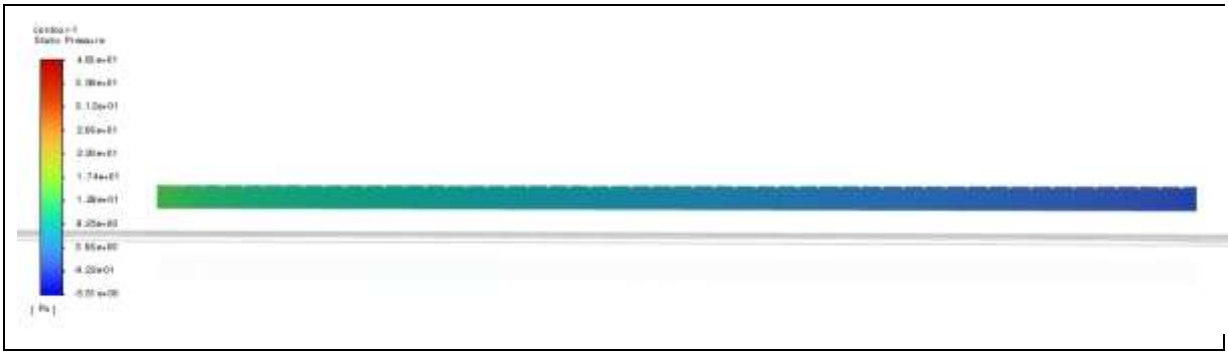

Figure 11: Pressure contour at Re=10000 of SAH duct with V-ribs axial air flow.

In the static pressure contours, different color codes represent varying magnitudes of static pressure from the inlet to the outlet of the duct. It's evident from Figure 10 and figure 11 that high pressure is observed at the inlet, gradually decreasing towards the outlet. This observation indicates the pressure distribution along the length of the duct, with the inlet exhibiting higher pressure levels compared to the outlet.

**3.3.2 Temperature contours**

Figure 12 and figure 13 shows the variation of static temperature along the length of smooth and roughened duct respectively. Both the figures are evident that there is a continuous increase in static temperature in both the cases. However more increase in temperature is obtained in roughened duct as compared to that of smooth duct.

ISSN PRINT 2319 1775 Online 2320 7876

 UGC CARE Listed ( Group -I) Journal Volume 11, Iss 01, 2022

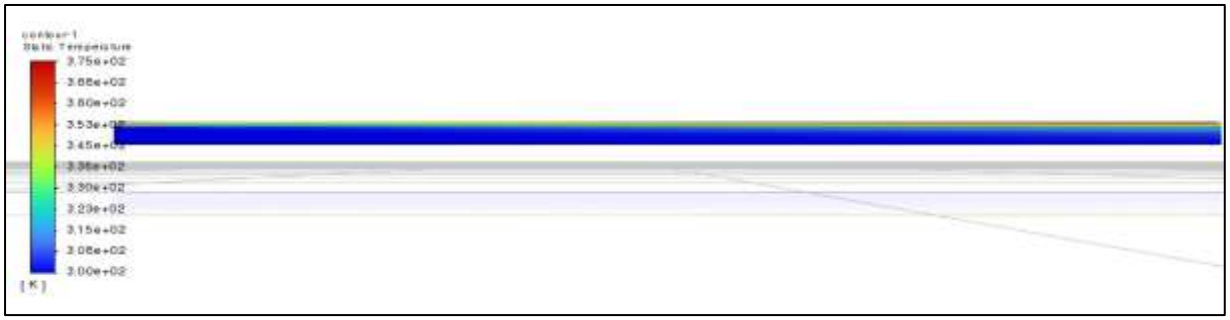

Figure 12: Temperature contour at Re=10000 of SAH Smooth duct axial air flow

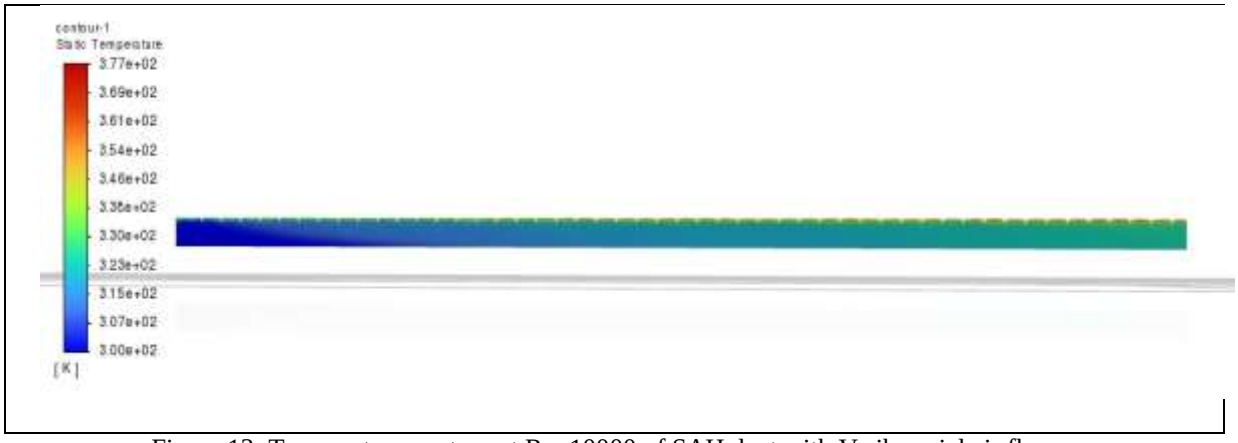


Figure 13: Temperature contour at Re=10000 of SAH duct with V-ribs axial air flow.

### 3.3.3 Velocity contours

Figure 14 and figure 15 shows the variation of velocity along the length of smooth and roughened duct respectively. Figure 14 shows that for a smooth duct there is a formation of boundary layer in both top and bottom side of the duct. However figure 15 is evident that there is disruption of boundary layer due to the presence of V-ribs at the top surface and boundary layer is still present on the bottom surface for roughened duct.

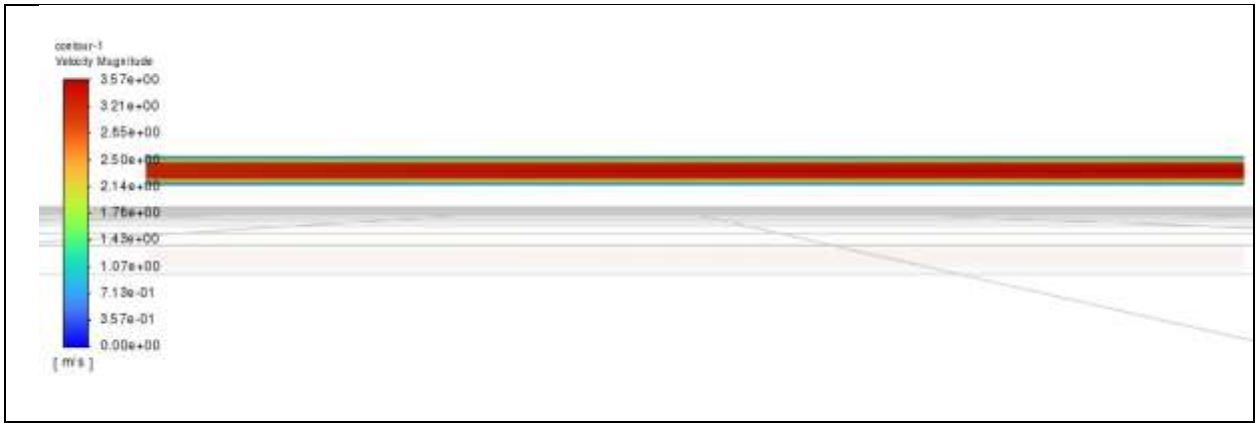


Figure 14: Velocity contour at Re=10000 of SAH Smooth duct axial air flow.

ISSN PRINT 2319 1775 Online 2320 7876

 UGC CARE Listed ( Group -I) Journal Volume 11, Iss 01, 2022

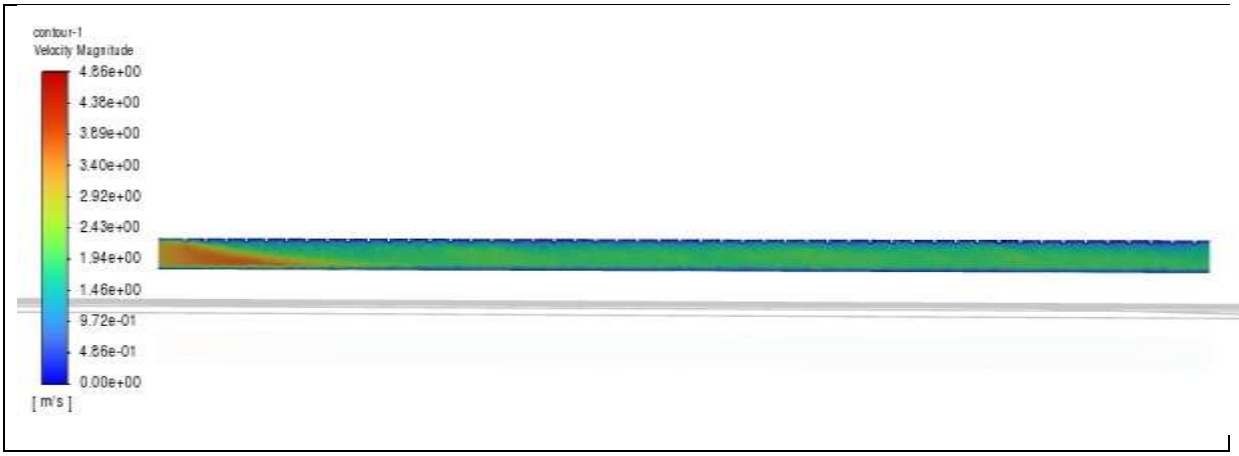


Figure 15:Velocity contour at Re=10000 of SAH duct with V-ribs axial air flow.

## 4. CONCLUSION

In the present study, we conducted a computational investigation into the impact of employing V-ribs as artificial roughness concerning the absorber plate of a Flat Plate Solar Air Heater (FPSAH) using ANSYS. The following conclusions can be inferred from our findings:

- As the Reynolds Number increases, subsequently boosting the mass flow rate through the Solar Air Heater (SAH), there is a noticeable rise in the Nusselt Number due to heightened turbulence levels.
- Increasing the Reynolds Number decreases the friction factor in both smooth and V-ribs roughened FPSAH. However, the pressure drop across the SAH increases with the rise in Reynolds Number.
- Utilizing V-ribs as artificial roughness yields higher Nusselt Numbers and friction factors compared to those of a smooth FPSAH, given the same Reynolds Number.
- Near the absorber plate, the temperature gradient is significant, while it approaches zero away from the plate at any cross-section along the FPSAH's length.
- Velocity gradients are evident near the walls of all FPSAH types due to the formation of boundary layers.
- Static pressure gradually decreases along the length of all FPSAH types due to frictional pressure losses.
- The hot outlet air is in the temperature range of 30 $^{0}$C to 80 $^{0}$C can be utilized for the drying of various foods, vegetables and grains.

## REFERENCE

[1] Sukhatme S. P., Nayak J. K. (2015), Solar Energy (3rd edition), Mc Graw Hill Education (India), ISBN-13: 978-0-07-026064-1.

[2] Kalogirou Soteris A (2014). Solar Energy Engineering (2nd edition), Academic Press is an Imprint of Elsevier, http://elsevier.com/locate/permissions.

[3] Hans VS, Saini RP, Saini JS. Heat transfer and friction factor correlations for a solar air heater duct roughened artificially with multi V-ribs. Sol Energy2010;84:898–911.

ISSN PRINT 2319 1775 Online 2320 7876

 UGC CARE Listed ( Group -I) Journal Volume 11, Iss 01, 2022

[4] Gupta D, Solanki SC, Saini JS. Heat and fluid flow in rectangular solar air heater ducts having transverse rib roughness on absorber plates. Sol Energy 1993;51:31–7.

[5] Saini RP, Saini JS. Heat transfer and friction factor correlations for artificially roughened ducts with expanded metal mesh as roughness element. Int J Heat Mass Transf 1997;40:973–86.

[6] Karwa R, Solanki SC, Saini JS. Thermo-hydraulic performance of solar air heaters having integral chamfered rib roughness on absorber plates. Energy2001;26:161–76.

[7] Lanjewar A, Bhagoria JL, Sarviya RM. Experimental study of augmented heat transfer and friction in solar air heater with different orientations of W-Rib roughness. Exp Therm Fluid Sci 2011;35:986–95.

[8] Jaurker AR, Saini JS, Gandhi BK. Heat transfer and friction characteristics of rectangular solar air heater duct using rib-grooved artificial roughness. Sol Energy2006;80:895–907.

[9] Karmare SV, Tikekar AN. Experimental investigation of optimum thermohydraulic performance of solar air heaters with metal rib grits roughness. Sol Energy2009;83:6–13.

[10] Aharwal KR, Gandhi BK, Saini JS. Experimental investigation on heat-transfer Enhancementdue to a gap in an inclined continuous rib arrangement in a rectangular duct of solar air heater. Renew Energy 2008;33:585–96.

[11] Saini SK, Saini RP. Development of correlations for Nusselt number and friction factor for solar air heater with roughened duct having arc-shaped wire as artificial roughness. Sol Energy 2008;82:1118–30.

[12] Saini RP, Verma J. Heat transfer and friction factor correlations for a duct having dimple-shape artificial roughness for solar air heaters. Energy 2008;33:1277–87.

[13] Bopche SB, Tandale MS. Experimental investigations on heat transfer and frictional characteristics of a turbulator roughened solar air heater duct. Int J Heat MassTransf 2009;52:2834–48.

[14] Ebrahim Momin A-M, Saini JS, Solanki SC. Heat transfer and friction in solar air heater duct with V-shaped rib roughness on absorber plate. Int J Heat Mass Transfer 2002;45:3383–96.

[15] Lanjewar A, Bhagoria JL, Sarviya RM. Heat transfer and friction in solar air heater duct with W-shaped rib roughness on absorber plate. Energy 2011;36:4531–41.

[16] Kumar A, Bhagoria J, Sarviya R. Heat transfer and friction correlations for artificially roughened solar air heater duct with discrete W-shaped ribs. Energy ConversManag 2009;50:2106–17.

[17] Singh I, Singh S. CFD analysis of solar air heater duct having square wave profiled transverse ribs as roughness elements. Sol Energy 2018;162:442–53.